

Nonlinear modeling of roof-to-wall connections in a gable-roof structure under uplift wind loads

Adnan F. Enajar^{1a}, Ryan B. Jacklin^{2b} and Ashraf A. El Damatty^{*1}

¹Department of Civil and Environmental Engineering, Faculty of Engineering, The University of Western Ontario, London Ontario Canada
²Tacoma Engineers, Guelph Ontario Canada

(Received February 6, 2018, Revised November 11, 2018, Accepted November 13, 2018)

Abstract. Light-frame wood structures have the ability to carry gravity loads. However, their performance during severe wind storms has indicated weakness with respect to resisting uplift wind loads exerted on the roofs of residential houses. A common failure mode observed during almost all main hurricane events initiates at the roof-to-wall connections (RTWCs). The toe-nail connections typically used at these locations are weak with regard to resisting uplift loading. This issue has been investigated at the Insurance Research Lab for Better Homes, where full-scale testing was conducted of a house under appropriate simulated uplift wind loads. This paper describes the detailed and sophisticated numerical simulation performed for this full-scale test, following which the numerical predictions were compared with the experimental results. In the numerical model, the nonlinear behavior is concentrated at the RTWCs, which is simulated with the use of a multi-linear plastic element. The analysis was conducted on four sets of uplift loads applied during the physical testing: 30 m/s increased by 5 m/s increments to 45 m/s. At this level of uplift loading, the connections exhibited inelastic behavior. A comparison with the experimental results revealed the ability of the sophisticated numerical model to predict the nonlinear response of the roof under wind uplift loads that vary both in time and space. A further component of the study was an evaluation of the load sharing among the trusses under realistic, uniform, and code pressures. Both the numerical model and the tributary area method were used for the load-sharing calculations.

Keywords: finite element method; wind load; roof-to-wall connections; wood structures; wind speed

1. Introduction

Since wood is a renewable and environmentally friendly resource, the majority of North American residences are wood structures. Severe hurricanes have seriously damaged a number of these wood houses. The Federal Emergency Management Agency (FEMA) has presented assessment reports of building performance under a series of hurricanes, such as Hurricane Andrew in 1992 and Hurricane Sandy in 2013. One of their findings is that the damage to light-frame wood structures observed in Florida following Hurricane Andrew was caused primarily by suction pressure on the roofs (FEMA 1992). Suction pressure causes damage to wood structures due to the inability of the wood connections to transfer this type of force to the ground (Morrison *et al.* 2014, Van de Lindt *et al.* 2007, Prevatt *et al.* 2012). Two critical connections have been observed in roof trusses: sheathing-to-truss connections (STTCs) and roof-to-wall connections (RTWCs) (Jacklin *et al.* 2014). These connections resist applied pressure through their withdrawal capacity, and each detail of the connections is associated with a different

withdrawal capacity. The differences arise from the varied types of nails used, such as common, box, and sinker nails, which have differing diameters and lengths (NDS 2015). Other types of connections, such as metal straps, provide higher levels of withdrawal capacity than common nails (Reed *et al.* 1997, Edmonson *et al.* 2012).

The withdrawal capacity of wood connections is dependent on the penetration depth of the nails and on the individual properties of the wood that forms the connections, such as water content and specific gravity (Luszczki *et al.* 2013). As a result, some connections are characterized by a higher degree of stiffness than others, and a stiffer connection can absorb a greater load. When a weak connection fails, the extra load is transferred to the adjacent connections, placing increased demands on the connections that have not yet failed (Guha and Kopp 2014). The consequence of any increases in the applied uplift load is that the remaining connections become unable to sustain that uplift load, resulting in additional connection failures.

The work presented in this paper was based on the use of the finite element model created by Jacklin (2013) for predicting the results of testing conducted at the Insurance Research Lab for Better Homes (IRLBH) located at the University of Western Ontario (Morrison *et al.* 2012). Because of the reasonable predictions it provides, finite element analysis is considered as an alternative tool for modeling light-frame wood houses subjected to wind loads. Kasal *et al.* (2004) studied the distribution of a lateral load on the walls of light-frame wood houses. Eight avenues of investigation were discussed in their study, including the tributary area, the total shear, the relative stiffness, and

*Corresponding author, Professor

E-mail: damatty@uwo.ca

^a Ph.D. Candidate

E-mail: aenajar@uwo.ca

^b M.Sc.

E-mail: rjacklin@gmail.com

three-dimensional finite element methods (FEM). Those methods were then applied for a determination of the lateral load sharing for each wall of a full-scale L-shaped experimental test house, with FEM producing the most accurate results. Thampi *et al.* (2011) used ANSYS commercial software to create a three-dimensional finite element model for evaluating tornado damage to a light-frame wood house located in Parkersburg, USA. The damage predicted by their model agreed well with that observed in the affected house. Shivarudrappa and Nielson (2013) investigated the load paths in light-frame wood structures under a wind uplift load by plotting the influence coefficient contours for each RTWC. For their study which was targeted at determining how the loads transferred vertically, they used ANSYS commercial software to develop a finite element model based on the experimental testing conducted by Datin *et al.* (2010). Zisis and Stathopoulos (2012) conducted three-dimensional finite element model using SAP2000 commercial software under real wind pressure evaluated by monitoring as-built gable-roof house. This model was used to validate the load cells at foundation level, and they found experimentally, that the foundation reaction was lower by an amount of 17% to 28% than predicted by the model. Satheskumar *et al.* (2017) evaluated numerically the effect of roof-cladding and roof-ceiling on the reaction of RTWCs by using FEM. In their model, they used ABAQUS commercial software based on the experimental testing performed by Satheskumar *et al.* (2016). It was concluded that there was a 25% reduction in the RTWCs uplift reactions by presence of these roof elements. From another perspective, Foschi (2000) established nail-connection element based on the elastoplastic behavior of the nail combined with nonlinear wood medium. This nail-connection element was implemented in finite element models of various components such as in wood shear walls (Minghao *et al.* 2012), and in 3D light-frame structures (He *et al.* 2001).

2. Numerical model

In the case of lightweight roof trusses, the connections between the trusses and the top plate have historically been toe-nailed, as shown in Fig. 1. Such connections are weak with respect to resisting wind-generated uplift forces. The capacity of toe-nail connections under uplift loads has been examined through tests conducted on a full-scale two-story gable roof house at the IRLBH (Morrison *et al.* 2012). The plane of this experimental house was approximately 9 m by 9 m with a roof pitch of 1:3. The roof of the house consisted of 16 trusses spaced 0.6 m apart, all having a roof overhang of 0.5 m in each direction. The middle 14 trusses were supported by two RTWCs on the north and south sides of the house while the remaining trusses were gable end trusses on the eastern and western sides, which were supported by walls as well as RTWCs on the north and south sides. On average, three twisted shank nails, either 12d or 16d, were used for each RTWC.

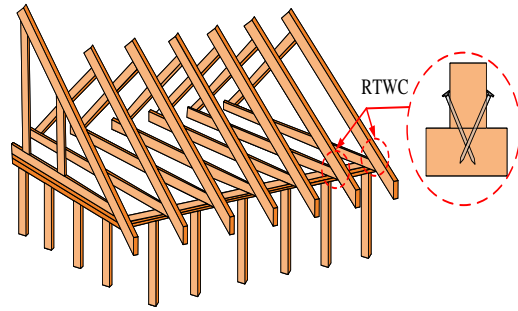


Fig. 1 Segment of a light-frame wood structure, with an inset view of a RTWC

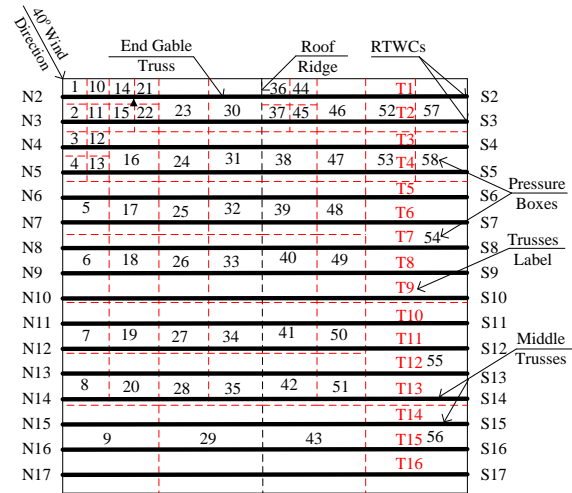


Fig. 2 Layout of the numerical model proposed by Jacklin (2013)

The wind load was simulated with the use of 58 pressure boxes that created suction pressure on the roof of the test house. To determine the appropriate pressure, a wind tunnel test was conducted as a means of establishing realistic wind loads, for which a 1:50 scale model was designed in order to measure realistic loads under flows from 18 wind directions across open terrain. Full-scale pressure was applied at a 40° angle because this pressure produces the greatest reaction generated on RTWCs. The experimental test was performed in six loading stages, ranging from hourly mean wind speed of 20 m/s up to complete failure of the roof at hourly mean wind speed of 45 m/s. All load steps were varied both spatially and temporally, with each load stage having a different loading period. Further details about the experimental test can be found in (Morrison *et al.* 2012).

Dessouki (2010) introduced a sophisticated numerical simulation using SAP 2000 commercial software, which was subsequently developed further by Jacklin (2013). The work presented in this paper was based on this latter version of the model, but the investigation has been expanded to cover the examination of more realistic wind loads in a nonlinear range associated with the occurrence of permanent withdrawal in the RTWCs. The dimensions and loading included in the new numerical model are similar to

those of the experimental gable roof house previously tested at the IRLBH (Morrison *et al.* 2012). As shown in Fig. 2, the new numerical model incorporates 16 Howe trusses modeled as frame elements, each of which has two nodes, with six degrees of freedom at each node. To increase the stiffness of the end trusses, four extra webs have been added. The top and bottom chords of the trusses are 2 in. by 4 in. (50 mm. by 101 mm.), and the webs are 2 in. by 3 in. (50 mm. by 76 mm.). All of the middle trusses are supported by two RTWCs except for the gable end trusses, which are assumed to be backed by seven RTWCs in order to simulate the bearing behavior of the end walls. The 9 mm roof sheathing is modeled using 2112 shell elements, each of which connected with all top truss chords by body constraints. These shell elements that have four nodes, with six degrees of freedom at each node (three translations and three rotations), which can capture both membrane and bending forces. The nonlinearity portion of the finite element model represents the nonlinear stiffness of the RTWCs, which are therefore modeled as nonlinear spring elements. Besides, there was an overhang of sheathing about 0.5 m in all directions. A rigid diaphragm was assigned at the level of top plate members. At that level, linear springs were allocated to account for the in-plane stiffness of the shear walls. This in-plane stiffness was estimated as linear approximation from the experimental testing conducted by Kasal *et al.* (1994).

As proposed by Morrison *et al.* (2012), when a connection exceeds the damage peaks evident in the displacement time history, that connection exhibits plastic behavior as a result of permanent withdrawal. For this reason, Jacklin (2013) used two types of nonlinear link elements for their RTWCs model: gap elements and multi-linear plastic elements. Gap elements carry only compression loads and were utilized in the model as a means of reducing negative deflection through the setting of a high degree of stiffness in compression. The second type of element addresses the tension forces generated from the suction pressure. To model this kind of behavior, the authors proposed a multi-linear load deflection relation with plastic kinematic hysteresis model, as shown in Fig. 3. This relationship was based on the nonlinear curve resulting from the experimental testing performed by Morrison and Kopp (2011). Experimentally, the load-deflection relation of toe-nailed RTWCs had high variability (Reed *et al.* 1997, Khan. 2012). However, the numerical model in this paper was carried out using an identical load-deflection relation for all RTWCs. In the case of hurricane clips connections, Chowdhury *et al.* (2013) and Satheeskumar *et al.* (2017) showed that the withdrawal capacity of these connections could be reduced due to the combination of lateral and uplift loading. However, the roof-to-wall connections used in this paper were toenails under the effect of wind uplift loads only. Morrison and Kopp (2011) stated that in case of roof pitch 1 to 3, the toenail connections received approximately 5% from the wind uplift loads as shear loads. The dominant failure of toenails is nail-withdrawal (Shanmugam *et al.*, 2009; Guha and Kopp 2014). The roof-to-wall connections herein were modeled as nonlinear spring elements. These elements accounted for the relative

deformation between the walls and the roof in the direction parallel to the toenails withdrawal. The other two directions were set to be rigid, so there was no relative deformation between the trusses and the walls in the directions perpendicular to the toenails withdrawal. The extra shear loads resulting from the resolution of the uplift loads will be resisted by the linear springs, which simulate the in-plane stiffness of the shear walls. Detailed information about the numerical model can be found in (Jacklin 2013).

3. Validation of the numerical model

To evaluate the performance of the numerical model against the experimental testing, the predicted RTWCs deflections were compared with the experimental results. The experimental data was too large, in the order of 30,000 data points for the 30 m/s wind speed and 20,000 data points for the 45 m/s wind speed. It was not practical to analyze the model nonlinearly under such large number of data points. So performing a complete numerical analysis for the full loading time history is computationally expensive. As a solution, the analysis focused on 1000 time steps within the range of maximum and minimum values of the loading at each velocity as shown in Fig.4. In Fig. 4 example, four data sets of realistic uplift wind load pressure values were applied in the numerical model. These demand data sets represent a variety of wind velocities, beginning with 30 m/s and increasing in 5 m/s increments up to complete roof failure at 45 m/s, when permanent withdrawal occurs in the RTWCs. For example, data set one represents the lowest percentage of permanent withdrawal of the RTWCs at 30 m/s, while data set four, at 45 m/s, correlates with maximum RTWCs withdrawal. All of the selected uplift wind load pressures thus produce plastic behavior in the connections. Based on the example shown in Fig. 4, the RTWC responses exhibit erratic fluctuations that correspond to loading peaks and unloading troughs. Plastic RTWC withdrawal occurs primarily at peak uplift pressure (Morrison *et al.* 2012). During the experimental results, especially in the nonlinear range of wind velocity between 30 m/s and 45 m/s, there was a permanent withdrawal in RTWCs (Morrison *et al.* 2012). And in order to compare the experimental results, the numerical prediction should be shifted up by the previous withdrawal in the whole time history, since the numerical analysis was based on initial zero deflection. The ability of the numerical model to predict accurately the incremental difference taking non-linear behavior into account is assessed.

The pressure applied on the roof of the house was varied both spatially and temporally so that the 58 pressure boxes created a different intensity at each time step. For example, the numerical model was analysed with the 20 sec intervals divided into 1000 time steps, each of which was associated with the spatial pressure values shown in Fig. 2. For the purposes of the nonlinear finite element analysis, the pressure is applied incrementally in a quasi-static time history manner under 1000 time steps. For example, step one includes the dead weight of the roof plus the spatial

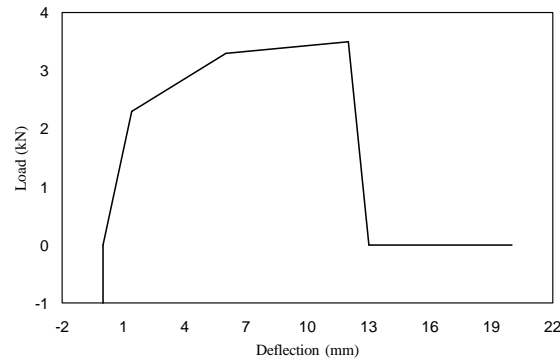


Fig. 3 Load-deflection relation for all connections, as proposed by Jacklin (2013)

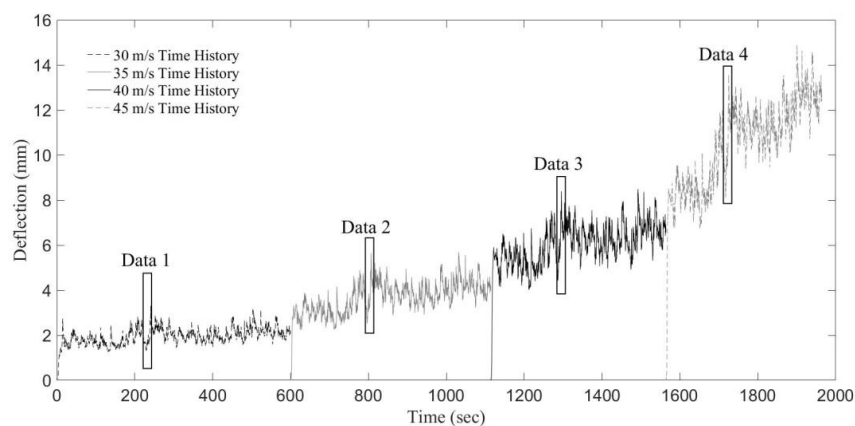


Fig. 4 Time history displacement for RTWC S6 (Morrison *et al.* 2012)

pressure associated with step one. Step two then begins with the initial step one condition plus the difference between the spatial pressure values associated with steps one and two, continuing in this manner until the analysis has been conducted for all of the time steps. This quasi-static analysis is also performed by Kumar *et al.* (2012) to assess the performance of gable roof house under tornado loading. In this paper, the analysis strategy is based on the assumption of an initial zero withdrawal in the first time step and does not take into account any previous withdrawal. Jacklin (2013) therefore proposed an approximated assumption for modifying the numerical analysis output by taking the differences between the experimental results and the numerical predictions at each RTWC for the first time step and then adding these differences to all time steps. This approximation is a reasonable prediction since the analysis is based on neglecting any previous plastic damage that occurred at the previous peaks in the pressure time history. The numerical model accounted for the dead weight of the structural members such as truss members, sheathings, and cross members between the trusses. However, the numerical model did not account for the weight of the non-structural elements such as roof-shingles since they were removed during the experimental testing as mentioned by Morrison *et al.* (2012).

Figs. 5 and 6 provide a comparison of the experimental results and the numerical deflection predictions with respect to the deflection of all of the RTWCs. The deflections were evaluated for four wind velocities: 30 m/s and 35 m/s (Fig. 5), and 40 m/s and 45 m/s (Fig. 6) under the effects of the ultimate applied pressure during the associated time history. As shown in Fig. 5, good agreement exists between the experimental deflections and the predicted deflections on the north and south sides in terms of magnitude and trend. With reference to the mean numerical values for wind velocities of 30 m/s and 35 m/s, the maximum differences between the experimental and the numerical deflection values are 0.3 mm and 0.4 mm, respectively, resulting in percentages of difference between the mean numerical and mean experimental values of 7.1% and 5.8%, respectively.

When the ultimate applied pressure increases with velocities above 35 m/s, the differences between the predicted numerical deflections and the experimental deflections increase, primarily on the south side under the maximum global uplift that corresponds to the 45 m/s failure velocity. These differences resulted mainly because a complete full-time history analysis was not performed, with the focus being only on the maximum and minimum uplift pressure values in data set four, as illustrated in Fig. 4. An additional factor was the fact that the analyses were based on a modification of the output numerical predictions

assumed by Jacklin (2013). However, as evidenced by Fig. 6, the output values are quite reasonable. For example, the maximum deflection differences between the experimental results and the finite element predictions are 3.8 mm and 5.8 mm for wind velocities of 40 m/s and 45 m/s, respectively. These differences result in percentage differences between the mean finite element predictions and the mean experimental results of 20.7 % and 23.6 % with reference to the mean numerical values for the 40 m/s and 45 m/s wind velocities, respectively.

Figs. 7 and 8 provide a comparison of the finite element predictions and the experimental test results for all RTWCs deflections on the north and south sides of the roof under the least amount of global uplift pressure for four wind velocities ranging from 30 m/s to 45 m/s. As shown in Fig. 7, the comparison reveals that both the numerical and the experiment curves exhibit the same trend. However, the deflection differences between the numerical predictions and the experimental results under the least uplift pressure are greater than the deflection differences under the maximum global uplift. With reference to the mean numerical values for pressures from wind velocities of 30 m/s and 35 m/s, these differences reach values of 0.6 mm and 0.5 mm, respectively, with percentages of difference between the mean numerical and the mean experimental deflection values of 17.7% and 13.6%, respectively.

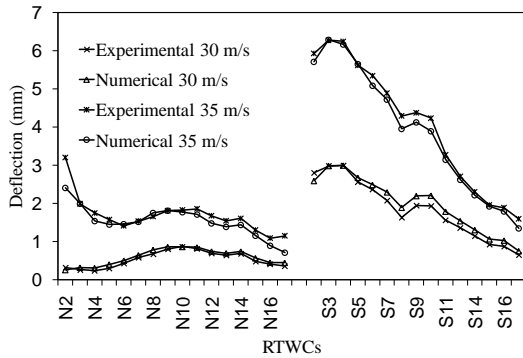


Fig. 5 Deflection values of RTWCs under maximum uplift pressure for wind velocities of 30 m/s and 35 m/s

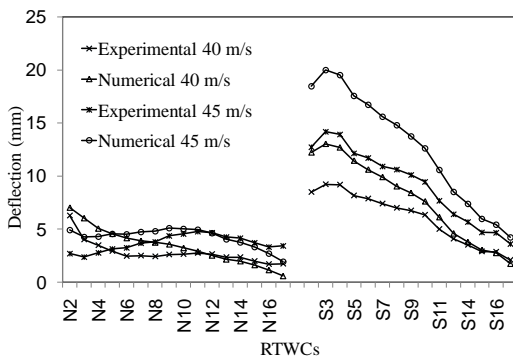


Fig. 6 Deflection values of RTWCs under maximum uplift pressure for wind velocities of 40 m/s and 45 m/s

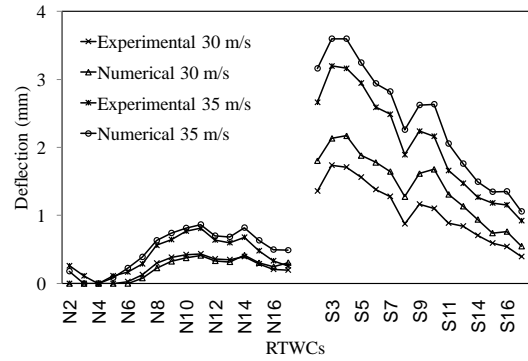


Fig. 7 Deflection values of RTWCs under minimum uplift pressure for wind velocities of 30 m/s and 35 m/s

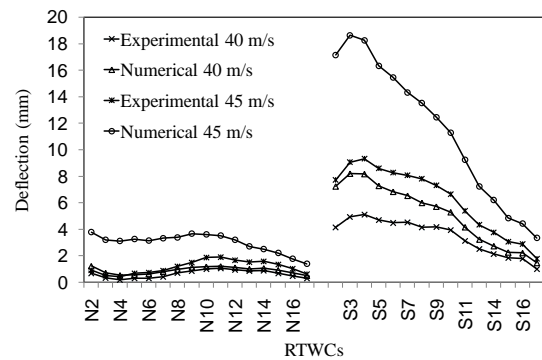


Fig. 8 Deflection values of RTWCs under minimum uplift pressure for wind velocities of 40 m/s and 45 m/s

A comparison of Figs. 5 and 7 reveals that both graphs indicate that the south side of the roof exhibits greater deflection than the north side due to the higher pressure intensity on the south side. Fig. 7 also shows zero deflection values for RTWCs N2 to N6, especially under the minimum pressure exerted by a wind velocity of 30 m/s. This happened when the self-weight of the roof was equal to the loads arising from the uplift pressure. As observed experimentally by Doudak *et al.* (2012), the tension and compression reactions were evaluated due to unsymmetrical gravity loads.

Fig. 8 shows the greatest variation recorded between the numerical and experimental test deflection values under minimum applied uplift pressure. With reference to the mean numerical values under pressure from wind velocities of 40 m/s and 45 m/s, the maximum differences recorded were 3.3 mm and 9.6 mm, respectively, with percentages of difference between the mean numerical and the mean experimental deflection values of 31.9 % and 49 %, respectively. However, this variation occurred because the same load-deflection curve shown in Fig. 3 was assumed in the numerical analysis, which does not represent the exact situation. Reed *et al.* (1997) conducted experimental testing on individual toe-nail connections and concluded that the coefficient of covariance for the ultimate uplift capacity reached about 25 %. As shown in Figs. 6 and 8, these variations in results have a significant effect on high-

velocity loads such as those at 40 m/s and 45 m/s, particularly in the nonlinear range associated with permanent withdrawal.

Figs. 9 and 10 illustrate the deflection values for RTWC S3 through the time history associated with pressure from four wind velocities ranging from 30 m/s to 45 m/s. Of all the RTWCs, RTWC S3 was observed to exhibit the greatest deflection measurements (Morrison *et al.* 2012). As shown in Fig. 9, good agreement exists between the numerical and the experimental deflection values with respect to the magnitude and shape of the curves. However, the maximum differences between the measured and expected deflections are 0.6 mm and 0.9 mm under the pressure of wind velocities of 30 m/s and 35 m/s, respectively.

At higher applied uplift pressures (wind speeds of 40 m/s and 45 m/s), the difference between measured and expected deflection values increased because the ultimate capacity or the failure of the RTWCs was reached. Fig. 10 indicates the differences between the experimental and numerical deflection values for RTWC S3 at the greater amounts of pressure from wind velocities of 40 m/s and 45 m/s. At the 40 m/s loading stage, good agreement exists during the first 2 sec, following which, the difference between the deflections is a maximum of 4 mm.

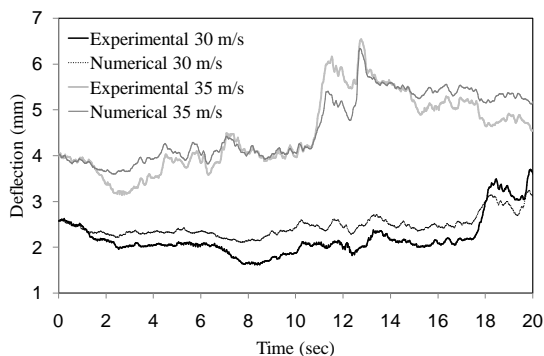


Fig. 9 Deflection values of RTWC S3 during the time history for wind velocities of 30 m/s and 35 m/s

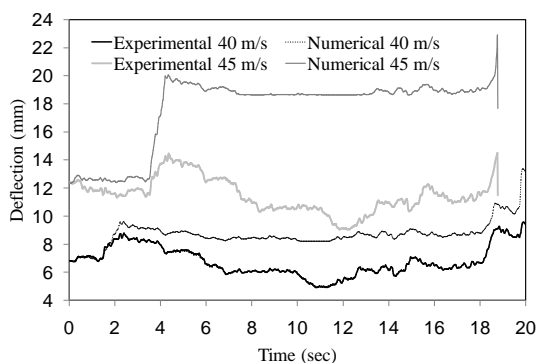


Fig. 10 Deflection values of RTWC S3 during the time history for wind velocities of 40 m/s and 45 m/s

For the failure uplift velocity of 45 m/s, the deflections during the first 4 sec reflect only small differences, and then an almost consistently greater difference in deflection is apparent, with a maximum value of 9.6 mm. From Fig. 10, it can be seen that the numerical model is able to capture the deflection that occurs between time step 1 and time step 938. The reason the analysis stops at time step 938 is that the total uplift predicted is greater than any of the RTWCs capacities. In summary, the output of the numerical model produces good prediction results following permanent withdrawal under velocities ranging from 30 m/s to 40 m/s. When the uplift load reaches failure, in this case, 45 m/s, the numerical model tends to overestimate the actual deflections. This overestimation is attributable to the similar stiffness values of the RTWCs used in the study, which, in reality, can vary depending on the nature of the wood connections.

4. Load sharing between trusses

Once the results produced by the numerical model had been validated against the experimental findings, the load sharing among the trusses could be evaluated in order to determine how the uplift load is transferred among them. Several experimental studies have been undertaken aimed to determining the load sharing throughout wood houses components. For example, Doudak *et al.* (2012) investigated the internal load transfer through gable roof house due to lateral and gravity loads. Moreover, Henderson *et al.* (2013) evaluated the change of Influence coefficients for each RTWCs under simulated uplift wind loads for hip roof house during permanent withdrawal of RTWCs. Datin and Prevatt (2013) estimated the influence functions for a small-scale gable-house by applying concentrated uplift loads on different locations at the roof in order to measure the reactions of the load cells located at RTWCs and at wall-to-foundation connections (WTFCs). The load share of each truss is defined herein as the ratio of the support reaction of each truss to the total uplift load. In this particular study, the self-weight of the roof is neglected so that the effects of the wind uplift loads could be compared separately. The load sharing was computed using both FEM (the numerical model) and the tributary area method for three load cases: realistic pressure, code pressure, and uniform pressure.

Fig. 11 illustrates the load sharing calculated by the numerical model for each truss under the realistic pressure derived from the experimental testing conducted by Morrison *et al.* (2012). Load sharing was also evaluated with respect to the maximum global uplift loads for a variety of wind velocities. It is clear from Fig. 11 that the gable end trusses, T1 and T16, are subject to a greater load share than the middle trusses. End gable truss T1, which is connected between RTWC N2 and RTWC S2, has 23.8 % and 19.5 % of the load share for wind velocities of 30 m/s and 45 m/s, respectively. End gable truss T16 extracts a lesser load share of 6.6 % and 9.5 % for wind velocities of 30 m/s and 45 m/s, respectively. The average load sharing by both end gable trusses for velocities varying from 30 m/s

up to 45 m/s is evaluated to be 29 %. This percentage is similar observation found by Zisis and Stathopoulos (2012). The reason that truss T1 is subjected to a greater load share than truss T16 can be attributed to the high degree of pressure intensity that occurs at truss T1 compared with that at truss T16, as shown in Fig. 13.

Fig. 13 indicates that the pressure distribution is more concentrated at truss T1 and that the pressure decreases gradually toward truss T16. In addition, the south side is subjected to greater pressure intensity than the north side. However, the north side also exhibits some peak pressure values that are concentrated on small box areas, such as boxes 10 and 14. For the maximum uplift wind load, Fig. 12 illustrates the load shares of all of the trusses except the gable end trusses. As shown in Fig. 12, the load sharing for all of the middle trusses under the pressure resulting from velocities of 30 m/s to 40 m/s follows the same trend, indicating that the RTWCs at these trusses do not reach their maximum capacity. However, at the failure wind velocity of 45 m/s, as given by Morrison *et al.* (2012), some of the middle trusses reach maximum capacity. The zero slope of the load sharing under the highest pressure at 45 m/s indicates that the RTWCs at trusses T2 to T8 reach their connection capacities and that roof failure is initiated in this zone.

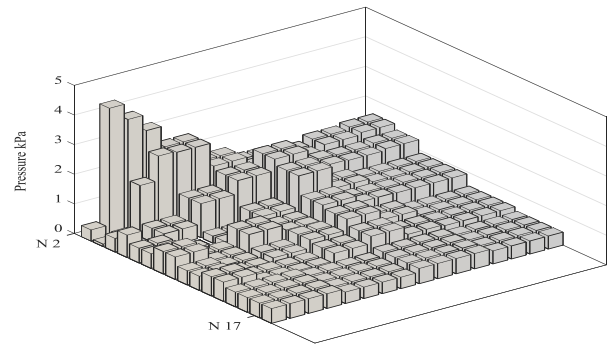


Fig. 13 Distribution of pressure over the roof under the maximum global uplift at 35 m/s (Morrison *et al.* 2012)

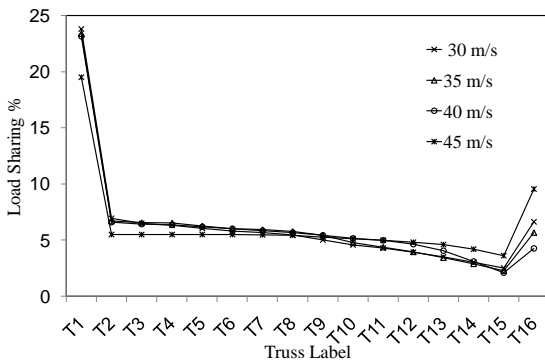


Fig. 11 FEM results indicating load sharing for all trusses at the maximum global uplift load

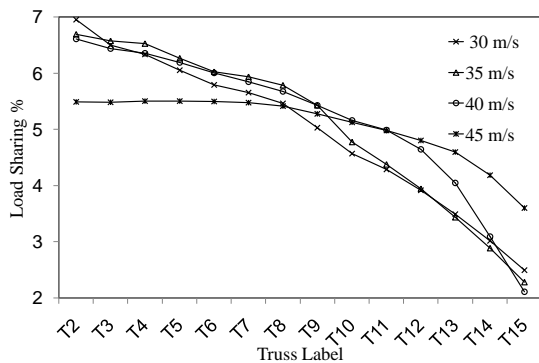


Fig. 12 FEM results indicating load sharing for all of the middle trusses at the maximum global uplift load

Instead of FEM, the tributary area method can be used for easily estimating approximate reactions at the RTWCs. With this approach, the pressure on the sheathing is distributed toward the nearest trusses based on the position of the trusses with respect to the pressure, rather than on the stiffness of the trusses. For example, if the pressure on the sheathing is supported by two trusses which have different degrees of stiffness, if the tributary area method is used, both trusses would share the same loading, which does not reflect the real situation. This method is thus reliant on the assumption that the horizontal diaphragm is flexible and that each truss works independently to transfer the loads towards the RTWC, as discussed by Kasal *et al.* (2004). In the study presented in this paper, the realistic pressure, as defined according to the 58 pressure boxes, whose layout is shown in Fig. 2, is distributed to all of the trusses. Each truss supports half of the pressure from the east and west sides as a line load, and this line load is then applied to the top chords of the trusses in order to obtain the reactions created in the RTWCs, which function as rigid supports.

Fig. 14 enables a comparison of the calculations of the load share by the numerical model and the tributary area method for end gable truss T1 under the effects of a wind speed of 40 m/s throughout the time history. As shown in Fig. 14, both analysis methods exhibit the same trend, with a constant average difference of 8%. The output from the tributary area method tends to represent an underestimation of the load sharing, a result that occurs for two reasons: first, the higher degree of stiffness in the gable end truss than in the middle trusses is not taken into account, and second, for the three-dimensional analysis, FEM includes consideration of the effects of outlying pressures on the reactions of all RTWCs. However, to sustain the equilibrium of the global uplift loads, the tributary area method provides greater estimated load shares in the middle trusses, such as truss T4, for example, where the average order of difference is 1.8%, as shown in Fig. 15. It should be noted that when the velocity is increased, the average difference does not vary greatly between the numerical model and the tributary area method results with respect to the load sharing among the trusses. For example, the average differences between the results produced by the numerical model and those calculated using the tributary area method are in the range of 7.1% and 9.0%,

respectively, for truss T1 and 1.3% and 2.0%, respectively, for truss T4.

Fig. 16 presents the results for the load sharing among the trusses under the pressure exerted by a wind velocity of 35 m/s, which represents the code pressure, as evaluated based on the National Building Code of Canada (2010). Four zones represent the uplift pressure: 2, 2E, 3, and 3E, with the greatest pressure at 2E in the northeast direction where the wind loads act on the structure as shown in Fig. 2. Open terrain exposure has been selected in order to obtain the pressure on the roof. Fig. 16 shows a comparison of the results using the numerical model and those computed using the tributary area method for evaluating the load sharing among the trusses. It can be seen that the tributary area method produces underestimates of the load shares at the gable end trusses by an average difference of 7.3% and overestimates of the load shares for the middle trusses by an average difference of 1.0%. These discrepancies arise with this method because the stiffness of the gable end trusses is not included in consideration. The load distribution evaluations produced by the tributary area method indicate a higher load share percentage allocated at trusses T2 to T9 than at the other middle trusses because the distribution is based on the intensity of the pressure. However, the load distribution determined using FEM shows less variation in the middle trusses than with the tributary area method, which indicates that the FEM distribution is reliant mainly on the stiffness of the intermediate trusses.

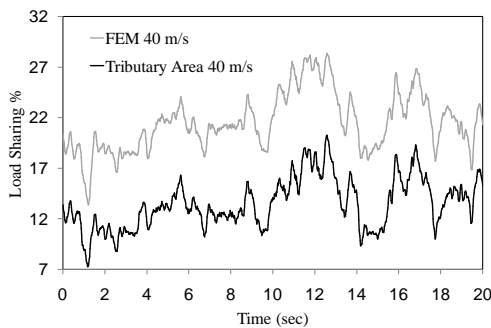


Fig. 14 Comparison of load sharing computed using the tributary area method and FEM predictions for end gable truss T1

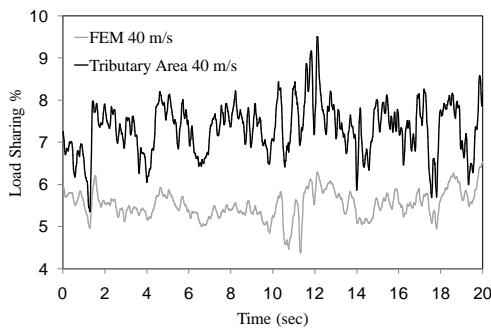


Fig. 15 Comparison of load sharing computed using the tributary area method and FEM predictions for middle truss T4

Fig. 17 shows the truss load shares calculated by the numerical model and the tributary area method under uniform pressure from a wind velocity of 35 m/s. The uniform pressure was evaluated as the weighted average of the 58 pressure boxes for the maximum global uplift at time step 633. The uniform pressure was utilized in order to identify the effect of truss stiffness on the load sharing when finite element analysis is used. As can be seen in Fig. 17, the numerical model calculated identical load shares for the end gable trusses due to these trusses having the same stiffness. Middle trusses with the same stiffness have slightly different load shares with symmetric elliptic shapes because of the flexural stiffness of the sheathing between the trusses. Otherwise, the tributary area method tends to compute the same load sharing at the middle trusses under uniform pressure, a result that is attributable to the use of similar widths for the trusses, with the exception of the gable end trusses, whose extra width accommodates the overhang.

Fig. 18 presents the output of the numerical model for two load cases: loads created by the maximum realistic pressure at time step 633, and loads under the code pressure. It can be seen that the two cases are characterized by similar load sharing at the middle trusses because both cases involve a graduated pressure distribution over the roof. However, differences appear with respect to the gable end trusses, where truss T1 is subjected to a greater load-sharing percentage than truss T16 when the maximum realistic pressure is applied.

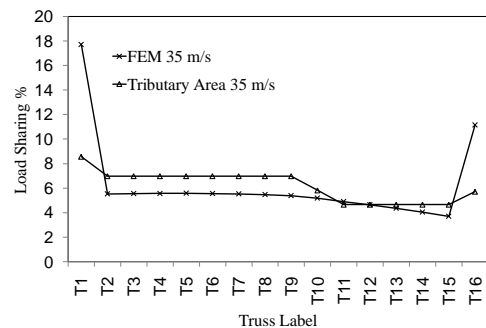


Fig. 16 Comparison of load sharing computed using the tributary area method and the FEM results under code pressure

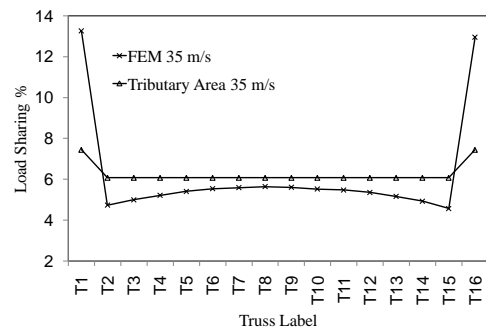


Fig. 17 Comparison of load sharing computed using the tributary area method and the FEM results under uniform pressure

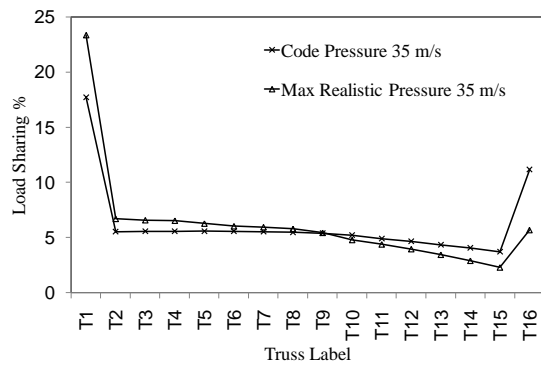


Fig. 18 Comparison of load sharing with the code pressure and the maximum realistic pressure obtained from FEM

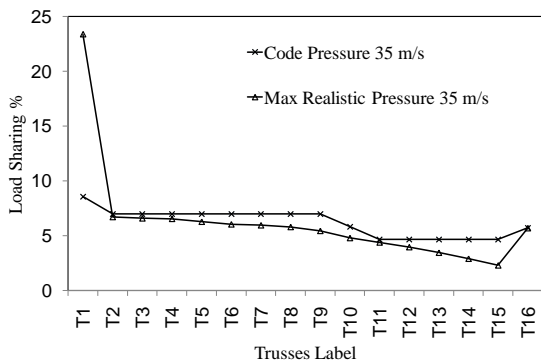


Fig. 19 Comparison of load sharing with the code pressure (tributary area method) and the maximum realistic pressure (FEM)

Fig. 19 provides a comparison of the results from two methods of evaluating the load sharing of the trusses: the tributary area method with the code pressure and the numerical model analysis with the maximum global applied realistic pressure. This comparison was conducted in order to assess the differences between simple analyses and more complicated ones. Fig. 19 reveals that the load sharing results obtained from both analyses are similar for all trusses but that the load share of end gable truss T1 is greater than that for truss T16 due to a combination of the greater pressure exerted at T1 and its higher degree of stiffness.

5. Conclusions

This paper has presented an examination of the use of both FEM and the simple tributary area method for the analysis of gable roof trusses subjected to uplift wind loads under the pressure of a variety of wind velocities. For the purposes of this study, three categories of pressure were considered: realistic pressure, code pressure, and uniform pressure. Realistic pressure, which varies with respect to time and space, was based on experimental testing

conducted at the Insurance Research Lab for Better Homes located at the University of Western Ontario (Morrison *et al.* 2012). The uniform pressure was established as a weighted average of each pressure box at the maximum global uplift load. The code pressure was estimated based on the National Building Code of Canada (2010).

The numerical model was validated against the experimental results under the realistic pressure in order to evaluate the performance of the predicted deflections at the RTWCs. Good agreement regarding the RTWCs deflections was obtained for minimum and maximum global uplift loads, especially at wind velocities of 30 m/s to 40 m/s. However, differences between the numerical and experimental deflections were observed under the pressure associated with the failure velocity of 45 m/s, with a maximum difference of 9.6 mm apparent at RTWC S3. This difference occurs due to the use of the same load-deflection relationship for all of the RTWCs. As discussed by Reed *et al.* (1997), the ultimate uplift capacity of toe-nail connections has a coefficient of covariance of about 25%, depending on the nature of the wood.

Values representing load sharing among the trusses were obtained from the numerical model for the pressure associated with maximum global uplift loads for a variety of wind velocities. Because of the higher degree of stiffness of the gable end trusses relative to the middle trusses and the greater windward pressure intensity, the load share of end gable truss T1 is greater than that of the other trusses, even end gable truss T16. At the failure velocity of 45 m/s, trusses T2 to T8 reach their maximum RTWC capacity at zero slopes on the load-sharing curve. Analysis performed using the tributary area method under the realistic pressure produces underestimates of the load shares of the gable end trusses because this method does not include consideration of the stiffness of the trusses. On the other hand, to sustain the equilibrium of the global uplift loads, the tributary area method produces overestimates of the load shares in the middle trusses.

Values obtained based on the code pressure reveal similar load sharing from the maximum global uplift wind load when finite element analysis is applied. However, a comparison of the load-sharing results provided by finite element analysis solved for the maximum global uplift loads and those resulting from the tributary area method analysis solved for the code pressure shows good agreement, with the exception of the results for the gable end truss on the windward side. Because the uniform load does not represent the spatial variations that characterize the true pressure situation, it was applied in the model only for an evaluation of the effect of truss stiffness.

References

- Chowdhury, A.G., Canino, I., Mirmiran, A., Suksawang, N. and Baheru, T. (2013), "Wind-loading effects on roof-to-wall connections of timber residential buildings", *J. Eng. Mech.*, **139**(3), 386-395.
- Datin, P.L., Mensah, A.F. and Prevatt, D.O. (2010), "Experimentally determined structural load paths in a 1/3-scale model of light-Framed wood, rectangular building",

- Proceedings of the 2010 ASCE Structures Congress*, Orlando, Florida, United States, May.
- Datin, P.L. and Prevatt, D.O. (2013), "Using instrumented small-scale models to study structural load paths in wood-framed buildings", *Eng. Struct.*, **54**, 47-56.
- Dessouki, A.A. (2010), "Analysis and retrofitting of low rise houses under wind loading", Master Thesis, University of Western Ontario, London, ON, Canada.
- Doudak, G., McClure, G. and Smith, I. (2012), "Experimental evaluation of load paths in light-frame wood structure", *J. Struct. Eng.*, **138**(2), 258-265.
- Edmonson, W.C., Schiff, S.D. and Nielson, B.G. (2012), "Behavior of light-framed wood roof-to-wall connectors using aged lumber and multiple connection mechanisms", *J. Perform. Constr. Fac.*, **26**(1), 26-37.
- FEMA (1992), *Building Performance: Hurricane Andrew in Florida, Observation, Recommendations, and Technical Guidance*, Federal Emergency Management Agency, Federal Insurance Administration, United States.
- Foschi, R.O. (2000), "Modeling the hysteretic response of mechanical connections for wood structures", *Proceedings of the 6th World Conf. on Timber Engineering*, Whistler, Canada, July.
- Guha, T.K. and Kopp, G.A. (2014), "Storm duration effects on roof-to-wall-connection failures of a residential, wood-frame, gable roof", *J. Wind Eng. Ind. Aerod.*, **133**, 101-109.
- He, M., Lam, F. and Foschi, R.O. (2001), "Modeling three-dimensional timber light-frame buildings", *J. Struct. Eng.*, **127**(8), 901-913.
- Henderson, D.J., Morrison, M.J. and Kopp, G.A. (2013), "Response of toe-nailed, roof-to-wall connections to extreme wind loads in a full-scale, timber-framed, hip roof", *Eng. Struct.*, **56**, 1474-1483.
- Jacklin, R.B. (2013), "Numerical and experimental analysis of retrofit system for light-framed wood structures under wind loading", Master Thesis, University of Western Ontario, London, ON, Canada.
- Jacklin, R.B., El Damatty, A.A. and Dessouki, A.A. (2014), "Finite-element modeling of a light-framed wood roof structure", *Wind Struct.*, **19**(6), 603-621.
- Kasal, B., Leichti, R.J., and Itani, R.Y. (1994), "Nonlinear finite-element model of complete light-frame wood structures", *J. Struct. Eng.*, **120**(1), 100-119.
- Kasal, B., Collins, M., Paevere, P. and Foliente, G. (2004), "Design models of light frame wood buildings under lateral loads", *J. Struct. Eng.*, **130**(8), 1263-1271.
- Khan, M.A.A. (2012), "Load-sharing of toe-nailed roof-to-wall connections under extreme wind loads in wood-frame houses", Master Thesis, University of Western Ontario, London, ON, Canada.
- Kumar, N., Dayal, V. and Sarkar, P.P. (2012), "Failure of wood-framed low-rise buildings under tornado wind loads", *Eng. Struct.*, **39**, 79-88.
- Luszczki, G.E., Clapp, J.D., Davids, W.G. and Lopez-Anido, R. (2013), "Withdrawal capacity of plain, annular shank, and helical shank nail fasteners in spruce-pine-fir lumber", *Forest Products J.*, **63**(5-6), 213-220.
- Minghao, L., Foschi, R.O. and Lam F. (2012), "Modeling hysteretic behavior of wood shear Walls with a Protocol-Independent Nail Connection Algorithm", *J. Struct. Eng.*, **138**(1), 99-108.
- Morrison, M.J., Kopp, G.A., Gavanski, E., Miller, C. and Ashton, A. (2014), "Assessment of damage to residential construction from the tornadoes in Vaughan, Ontario, on 20 August 2009", *Can. J. Civil Eng.*, **41**, 550-558.
- Morrison, M.J., Henderson, D.J. and Kopp, G.A. (2012), "The response of a wood-frame, gable roof to fluctuating wind loads", *Eng. Struct.* **41**, 498-509.
- Morrison, M.J. and Kopp, G.A. (2011), "Performance of toe-nail connections under realistic wind loading", *Eng. Struct.*, **33**, 69-76.
- NBCC (2010), *User's Guide--NBC 2010: Structural Commentaries (Part 4 of Division B)*, Canadian Commission on Building and Fire Codes, National Research Council Canada, and Institute for Research in Construction (Canada), Ottawa, ON, Canada.
- NDS (2015), *National Design Specification for Wood Construction*, American Wood Council, Leesburg, Virginia, USA.
- Prevatt, D.O., van de Lindt, J.W., Back, E.W., Graettinger, A.J., Pei, S., Coulbourne, W., Gupta, R., James, D. and Agdas, D. (2012), "Making the case for improved structural design: tornado outbreaks of 2011", *Leadership Manage. Eng.*, **12**(4), 254-270.
- Reed, T.D., Rosowsky, D.V. and Schiff, S.D. (1997), "Uplift capacity of light-frame rafter to top plate connections", *J. Architect. Eng.*, **3**(4), 156-163.
- Satheeskumar, N., Henderson, D.J., Ginger, J.D. and Wang, C. (2017), "Three-dimensional finite-element modeling and validation of a timber-framed house to wind loading", *J. Struct. Eng.*, **143**(9), 04017112.
- Satheeskumar, N., Henderson, D.J., Ginger, J.D. and Wang, C.H. (2017), "Finite element modelling of the structural response of roof to wall framing connections in timber-framed houses", *Eng. Struct.*, **134**, 25-36.
- Satheeskumar, N., Henderson, D.J., Ginger, J.D., Humphreys, M.T. and Wang, C.H. (2016), "Load sharing and structural response of roof-wall system in a timber-framed house", *Eng. Struct.*, **122**, 310-322.
- Shivarudrappa, R. and Nielson, B.G. (2013), "Sensitivity of load distribution in light-framed wood roof systems due to typical modeling parameters", *J. Perform. Constr. Fac.*, **27**(3), 222-234.
- Thampi, H., Dayal, V. and Sarkar, P.P. (2011), "Finite element analysis of interaction of tornados with a low-rise timber building", *J. Wind Eng. Ind. Aerod.*, **99**(4), 369-377.
- Van de Lindt, J.W., Graettinger, A., Gupta, R., Skaggs, T., Pryor, S. and Fridley, K.J. (2007), "Performance of wood-frame structures during hurricane katrina", *J. Perform. Constr. Fac.*, **21**(2), 108-116.
- Zisis, I. and Stathopoulos, T. (2012), "Wind load transfer mechanisms on a low wood building using full-scale load data", *J. Wind Eng. Ind. Aerod.*, **104-106**, 65-75.

CC